

Simulation of Three Dimensional Progressive Damage in Composite Laminates

Ali Evcil

Abstract— A three-dimensional, non-linear finite element code was developed to simulate the progressive damage of composite laminates in three dimensional space and to analyze the failure propagation and mode of failure around composite to metal joints. The code includes large displacement theory, isotropic and orthotropic material properties and a contact algorithm based on transformation matrix. A progressive damage model was implemented to predict the extent and the failure modes of the internal damage in composite laminates as a function of applied load and to stimulate the three-dimensional response of composite laminates from initial loading to final collapse. Hashin failure criteria was used together with the fiber-matrix shear failure and Yeh delamination criterion and material properties were degraded according to the mode of failure.

3D non-linear finite element formulation was tested with a 45° bend cantilever provided with a concentrated tip load and a solid sphere with radius $R = 1.0$ cm compressed diametrically by two parallel rigid plates was modeled to verify the contact algorithm. The progressive damage algorithm was verified using a clustered cross-ply $[0_6/90_6]_s$ laminate with a hole under compressive in-plane load. The results determined were found to be in good agreement with the experimental results with a deviation of as low as 2.6 % from the average.

Pinned joint failure analysis of same cross-ply $[0_6/90_6]_s$ laminate was conducted using two different geometries and net-tension, bearing, shear-out and mixed modes of failure of the joined was examined according to the progression of the damage.

Keywords— Composite Materials, Finite Element Analysis, Pinned Joints, Progressive Damage

I. INTRODUCTION

IN recent years, fiber reinforced composite materials have been used extensively in various engineering structural designs, especially in aerospace and defense industries, due to their high strength to weight ratio. In these structural applications, composite laminates are generally connected either to composites or to metals by mechanical means, including the joints like pinned or bolted joints. These joints cause stress concentrations since they form a discontinuity in the structure. For reliability assurance, stress and failure analysis of such structures, especially at the locations of stress concentration, have thus become an important subject of research.

Manuscript received Aug. 26, 2007; Revised version received Dec. 12, 2007.

A. Evcil is with the Mechanical Engineering Department, Near East University, Nicosia, Cyprus (e-mail: evcil@neu.edu.tr).

Out-of-plane loads play an essential role in the failure analysis making it desirable to conduct a three-dimensional analysis for failure prediction of such joints.

Mode of failure and failure propagation is another area of interest, since it may be useful in the improvement of the design, including the material and the structural design.

The aim of this study is to develop a three-dimensional failure analysis methodology for the analysis of composite laminates and to extend it further composite to metal joints. For this purpose, finite element method was used. A three-dimensional finite element code was developed including linear isotropic and linear orthotropic material properties, linear and geometrically non-linear stress analysis, contact stress analysis, failure criteria, which can predict the mode of failure, and property degradation rules.

It is expected to find the first ply and catastrophic failure loads of composite laminates at critical parts like discontinuities and joints. The failure modes and the propagation of the damage will also be observed that can be useful during the improvement of a design.

II. IMPLEMENTATION AND VERIFICATION OF 3D PROGRESSIVE DAMAGE CODE

A. 3D Non-Linear Finite Element Formulation

Three dimensional, 8-noded, isoparametric solid elements [1,2] were used during the implementation of the finite element program. The formulation was based on total Lagrangian method [3] so that large rotations and finite strains can be utilized. Full tangential stiffness matrix for total Lagrangian formulation can be written as;

$$\mathbf{K}_t = \mathbf{K}_{t1} + \mathbf{K}_{t\sigma} = \int (\mathbf{B}_{nl}^T(\mathbf{p})\mathbf{C}_t\mathbf{B}_{nl}(\mathbf{p}) + \mathbf{G}^T\hat{\mathbf{S}}\mathbf{G})dV_o$$

where

\mathbf{K}_{t1} : linear part of tangential elemental stiffness matrix

$\mathbf{K}_{t\sigma}$: geometrical or initial stress contribution to the tangential elemental stiffness matrix

\mathbf{B}_{nl} : non-linear strain-displacement transformation matrix

\mathbf{C}_t : material stiffness matrix

$\hat{\mathbf{S}}$: second Piolla-Kirchhoff stresses

\mathbf{G} : matrix relating vector of nodal displacements to displacement derivative tensor.

Full tangential stiffness matrix of the above equation was calculated by using Gaussian integration technique with full Newton–Raphson iterations [2,4]. Imposing the boundary conditions and solving for displacements, Green strain tensor can be determined which is the conjugate with the second Piolla-Kirchhoff stress tensor from which Cauchy stresses can be calculated.

The formulation was tested with a 45° bend cantilever provided with a concentrated load as introduced by Bathe [5], who used 16-node solid elements, by Slavkovic [6], who used enhanced three-dimensional elements and by Klinkel [7], who used three-dimensional brick elements with enhanced assumed strains. The bend has a radius of 2540 mm (100 in) and a cross-section of 25.4 mm x 25.4 mm (1.0 in x 1.0 in).

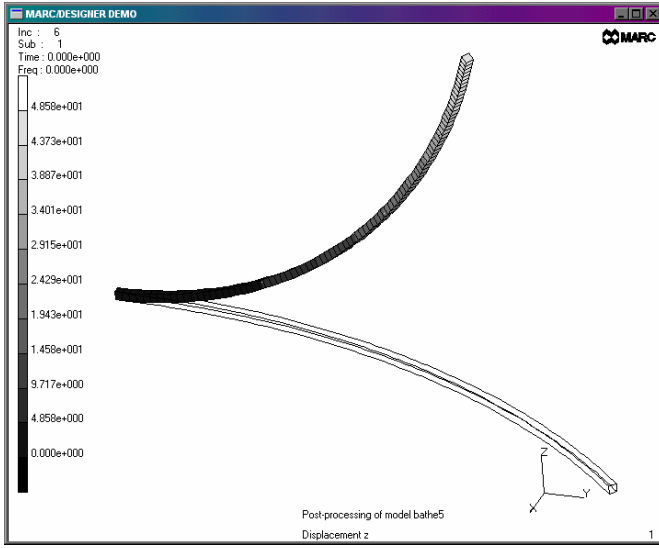


Fig. 1. Displacements in z-direction at F = 2670 N of 3D large deflection isotropic analysis of a 45° circular bend.

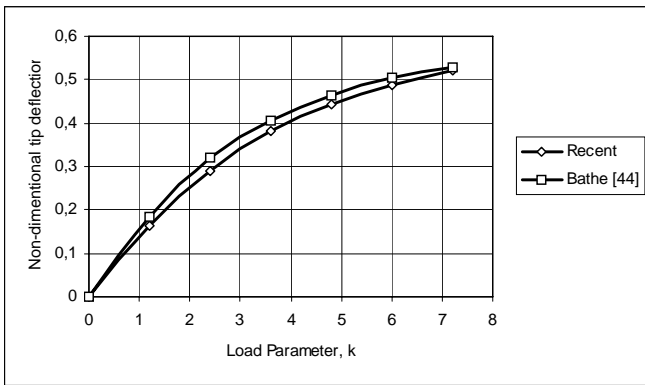


Fig. 2. Non-dimensional tip deflection, w/R vs. load parameter, $k=PR^2/EI$.

To check for convergence, the cantilever was analyzed using 15, 30, 60, 90 and 160 elements along the beam and a single element for the cross-section. One end of the model was fixed in all directions and 2670 N (600 lb) force was applied incrementally in z-direction in 6 increments. The

initial and final deformed geometry for 160 elements can be seen in Fig.1 with a maximum deformation of 1234 mm (48.58 in) at the tip. The comparison of results can be seen in Fig.2 and said to be in good agreement with the analysis of Bathe [5].

B. Isotropic and Orthotropic Material Properties

Material stiffness matrix for an isotropic material can be given as [8,9];

$$[C] = \frac{E}{(1+\nu)(1-2\nu)} \begin{bmatrix} 1-\nu & \nu & \nu & 0 & 0 & 0 \\ \nu & 1-\nu & \nu & 0 & 0 & 0 \\ \nu & \nu & 1-\nu & 0 & 0 & 0 \\ 0 & 0 & 0 & \frac{1-2\nu}{2} & 0 & 0 \\ 0 & 0 & 0 & 0 & \frac{1-2\nu}{2} & 0 \\ 0 & 0 & 0 & 0 & 0 & \frac{1-2\nu}{2} \end{bmatrix}$$

where E is the Young’s modulus and ν is the Poisson’s ratio. Material stiffness matrix for an orthotropic material can also be given as;

$$[C] = \begin{bmatrix} C_{11} & C_{12} & C_{13} & 0 & 0 & 0 \\ C_{12} & C_{22} & C_{23} & 0 & 0 & 0 \\ C_{13} & C_{23} & C_{33} & 0 & 0 & 0 \\ 0 & 0 & 0 & C_{44} & 0 & 0 \\ 0 & 0 & 0 & 0 & C_{55} & 0 \\ 0 & 0 & 0 & 0 & 0 & C_{66} \end{bmatrix}$$

where

$$C_{11} = \frac{1-\nu_{23}\nu_{32}}{E_2E_3\Delta}, \quad C_{22} = \frac{1-\nu_{13}\nu_{31}}{E_1E_3\Delta}, \quad C_{33} = \frac{1-\nu_{12}\nu_{21}}{E_1E_2\Delta}$$

$$C_{12} = \frac{\nu_{21} + \nu_{31}\nu_{23}}{E_2E_3\Delta} = \frac{\nu_{12} + \nu_{32}\nu_{13}}{E_1E_3\Delta}$$

$$C_{13} = \frac{\nu_{31} + \nu_{21}\nu_{32}}{E_2E_3\Delta} = \frac{\nu_{13} + \nu_{12}\nu_{23}}{E_1E_2\Delta}$$

$$C_{23} = \frac{\nu_{32} + \nu_{12}\nu_{31}}{E_1E_3\Delta} = \frac{\nu_{23} + \nu_{21}\nu_{13}}{E_1E_2\Delta}$$

$$C_{44} = G_{23}, \quad C_{55} = G_{31}, \quad C_{66} = G_{12}$$

$$\Delta = \frac{1-\nu_{12}\nu_{21}-\nu_{23}\nu_{32}-\nu_{31}\nu_{13}-2\nu_{21}\nu_{32}\nu_{13}}{E_1E_2E_3}$$

E_i : Young’s modulus in i directions.

ν_{ij} : Poisson’s ratio for transverse strain in the j -direction when stress is in the i -direction.

G_{ij} : Shear modulus in i - j plane.

C. Considerations in 3D Contact Analysis

A contact search algorithm to find the nodes coming into contact and a contact analysis to simulate the contact of pin and laminate were implemented to the computer code. In general, in three-dimensional contact problems, contact bodies

are denoted as contactor and target. The target surface can be discretized into several piecewise smooth triangular surfaces. Node E is the typical contact node of contactor and the triangle surface 1-2-3 is the typical target surface as shown in Fig.3. From the contact conditions, the nodes on the contactor should not penetrate the target surface and no tensile nodal forces exist on those nodes.

The displacement of node E on the surface of contactor, $\{\Delta q_{E \rightarrow e}\}$, can be treated as the combination of gap displacement, $\{\Delta q_{E \rightarrow F}\}$, sticking displacement, $\{\Delta q_{E \rightarrow f}\}$, relative sliding displacement, $\{\Delta q_{f \rightarrow e}\}$.

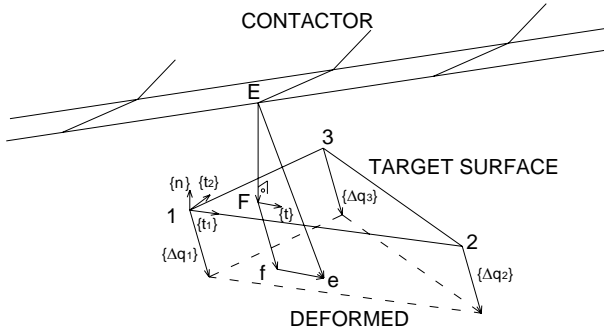


Fig.3. Kinematic conditions of contact surface

The point F is the initial contact point on the target surface. If the relative sliding displacement $\{\Delta q_{f \rightarrow e}\}$ is a zero vector, node E is a sticking node. Otherwise, node E is a sliding node.

For each non-contacting node of contactor, in general, there are three displacement components to be determined. If a node is known to be in sticking contact since the gap vector is known, its displacement can be determined by the deformation of the target surface and no independent unknowns exist. If a node is found to be in sliding contact, only the parameters Δq_{s1} and Δq_{s2} are left as the independent unknowns. The parameters Δq_{s1} and Δq_{s2} represent the magnitude of relative sliding displacements along $\{t_1\}$ and $\{t_2\}$ which are arbitrarily chosen two perpendicular unit tangential vectors on the triangular surface. Thus, the number of independent unknowns for each node of contactor can be 0, 2 or 3, depending on its contact condition. For detailed formulation of the contact algorithm it can be referred to [10].

For contact search, it is assumed that, if a node is in the contact control volume below the target segments surface of certain height the node comes in contact with the element.

For the verification of contact algorithm, a solid sphere with radius $R = 1.0$ cm compressed diametrically by two parallel rigid plate was examined as discussed by Chen and Yeh [10]. Due to symmetry, only one-eighth of the sphere was modeled. An incremental downwards displacement was given from the upper edge of the model. The Young modulus and Poisson's ratio of the sphere were taken to be 1000 N/cm^2 and 0.3, respectively. The contact surface was considered to be frictionless.

Distribution of normal stress can be seen in Fig.4 with a maximum stress of 165 N/cm^2 . In Fig.5, distribution of normal contact tractions along x-axis is shown. There is a numerical oscillation at the initial contact point ($x = 0$) due to mesh size and caused an error in contact traction diminishing towards the end of the contact area.

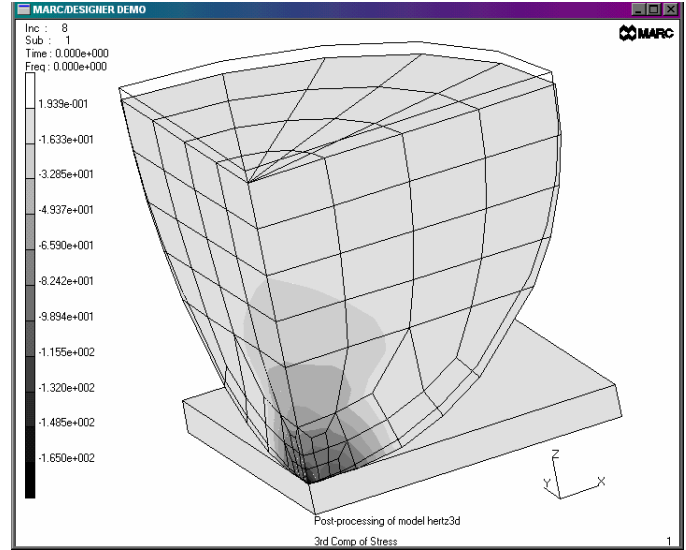


Fig.4. Normal Stress Distribution

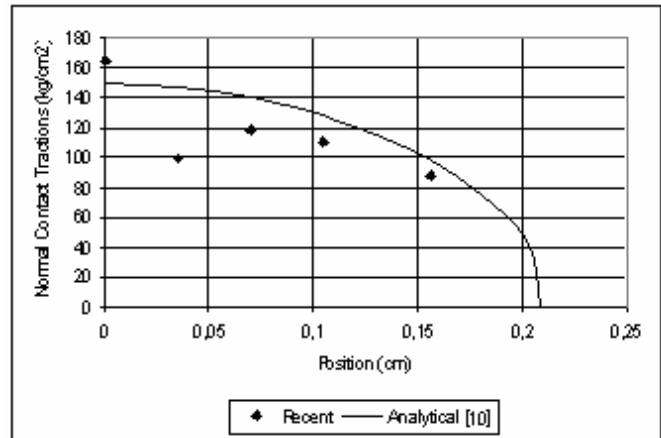


Fig.5. Distribution of Normal Contact Tractions Along x-axis

D. Failure Theory

Hashin [11] type failure criterion is ideal for use in finite element models, especially when adapted to progressive damage models since it has distinct polynomials corresponding to different failure modes. It combines the advantage of accuracy found in the polynomial criteria and the ability to distinguish failure mode. It has been found wide application in different studies. [12,13] Hashin failure criterion is summarized below.

Tensile Fiber Failure Mode

$$\left(\frac{\sigma_{11}}{\sigma_A^+}\right)^2 + \frac{1}{\tau_A^2}(\sigma_{12}^2 + \sigma_{13}^2) = 1 \text{ for } \sigma_{11} > 0$$

Compressive Fiber Failure Mode

$$\sigma_{11} = -\sigma_A^- \text{ for } \sigma_{11} < 0$$

Tensile Matrix Failure Mode

$$\frac{1}{\sigma_T^{+2}}(\sigma_{22} + \sigma_{33})^2 + \frac{1}{\tau_T^2}(\sigma_{23}^2 - \sigma_{22}\sigma_{33}) + \frac{1}{\tau_A^2}(\sigma_{12}^2 + \sigma_{13}^2) = 1$$

for $\sigma_{22} + \sigma_{33} > 0$

Compressive Matrix Failure Mode

$$\frac{1}{\sigma_T^-} \left[\left(\frac{\sigma_T^-}{2\tau_T} \right)^2 - 1 \right] (\sigma_{22} + \sigma_{33}) + \frac{1}{4\tau_T^2} (\sigma_{22} + \sigma_{33})^2 + \frac{1}{\tau_T^2} (\sigma_{23}^2 - \sigma_{22}\sigma_{33}) + \frac{1}{\tau_A^2} (\sigma_{12}^2 + \sigma_{13}^2) = 1$$

for $\sigma_{22} + \sigma_{33} < 0$

In addition to Hashin failure criterion, fiber-matrix shearing failure and Yeh delamination criterion can also be used during the failure analysis and can be given as

Fiber-Matrix Shearing Failure [14]

$$\left(\frac{\sigma_{11}}{\sigma_A^-}\right)^2 + \left(\frac{\sigma_{12}}{\tau_A}\right)^2 = 1 \text{ for } \sigma_{11} < 0$$

Yeh Delamination Criterion [15]

$$\left(\frac{\sigma_{33}}{\sigma_T^+}\right)^2 + \left(\frac{\sigma_{13}}{\tau_A}\right)^2 + \left(\frac{\sigma_{23}}{\tau_T}\right)^2 = 1 \text{ for } \sigma_{33} > 0$$

or

$$\left(\frac{\sigma_{13}}{\tau_A}\right)^2 + \left(\frac{\sigma_{23}}{\tau_T}\right)^2 = 1 \text{ for } \sigma_{33} < 0$$

where;

σ_{ij} : Components of stress tensor,

σ_A^+ : Tensile failure stress in fiber direction,

σ_A^- : Compressive failure stress in fiber direction (absolute value),

σ_T^+ : Tensile failure stress transverse to fiber direction,

σ_T^- : Compressive failure stress transverse to fiber direction (absolute value),

τ_T : Shear stress corresponding to transverse failure,

τ_A : Shear stress corresponding to axial failure.

E. Progressive Damage and Degradation Rules

In the progressive damage analysis, the load is applied incrementally and the stress-strain distributions are determined in each increment [16]. Every element is checked for failure. If there is no failure the next load step is performed. In case of failure, the material properties of that element are degraded. Stresses are then redistributed at the same load and re-examined for any additional failure. Convergence at a load step without additional failure allows the next load step to be performed and the procedure continues until a point where excessive damage is reached (catastrophic failure). A general algorithm for progressive damage analysis is shown in Fig.6.

The material properties of failed elements must be degraded according to the mode of failure. Different degradation coefficients can be observed in different studies and failure modes ranging between 0 to 0.4 [12,13,17].

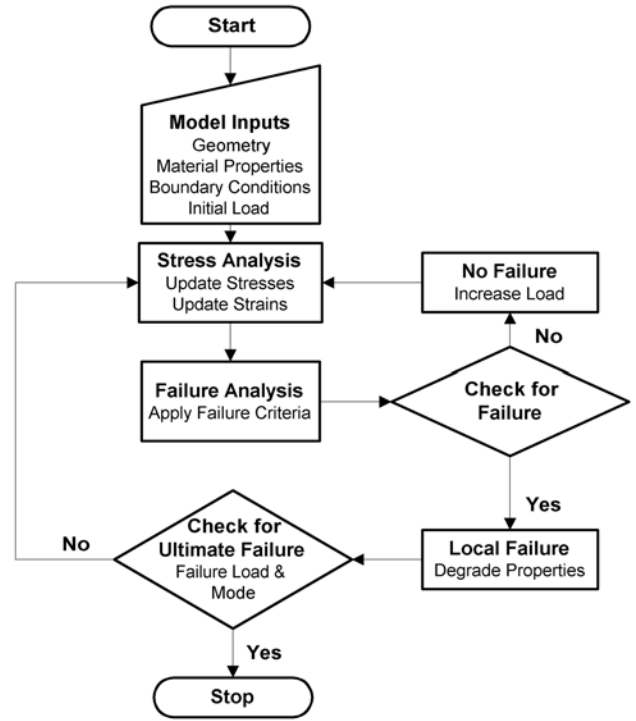


Fig.6. Algorithm for progressive damage analysis.

In this study, in tensile and compressive fiber failure modes it will be assumed that the material loses all its properties, therefore, the elements of the orthotropic material properties matrix becomes all zero:

$$[C] \rightarrow \begin{bmatrix} 0 & 0 & 0 & 0 & 0 & 0 \\ 0 & 0 & 0 & 0 & 0 & 0 \\ 0 & 0 & 0 & 0 & 0 & 0 \\ 0 & 0 & 0 & 0 & 0 & 0 \\ 0 & 0 & 0 & 0 & 0 & 0 \\ 0 & 0 & 0 & 0 & 0 & 0 \end{bmatrix}$$

However, in order to avoid numerical problems, the matrix will not be equated to zero but to a very small number.

If the matrix fails due to tensile or compressive loading, the material loses its transverse properties and Poisson's effect. The material properties degrade as follows.

$$[C] \rightarrow \begin{bmatrix} E_1 & 0 & 0 & 0 & 0 & 0 \\ 0 & 0 & 0 & 0 & 0 & 0 \\ 0 & 0 & 0 & 0 & 0 & 0 \\ 0 & 0 & 0 & G_{12} & 0 & 0 \\ 0 & 0 & 0 & 0 & G_{23} & 0 \\ 0 & 0 & 0 & 0 & 0 & G_{13} \end{bmatrix}$$

If the failure mode is fiber-matrix shearing mode, then the material loses its shear properties and the Poisson's effect. The material properties degrade as follows.

$$[C] \rightarrow \begin{bmatrix} E_1 & 0 & 0 & 0 & 0 & 0 \\ 0 & E_2 & 0 & 0 & 0 & 0 \\ 0 & 0 & E_3 & 0 & 0 & 0 \\ 0 & 0 & 0 & 0 & 0 & 0 \\ 0 & 0 & 0 & 0 & 0 & 0 \\ 0 & 0 & 0 & 0 & 0 & 0 \end{bmatrix}$$

If delamination causes the failure, then the material loses its properties in the thickness direction, Poisson's effect and will not be able to carry shear loads. The material properties degrade as follows.

$$[C] \rightarrow \begin{bmatrix} E_1 & 0 & 0 & 0 & 0 & 0 \\ 0 & E_2 & 0 & 0 & 0 & 0 \\ 0 & 0 & 0 & 0 & 0 & 0 \\ 0 & 0 & 0 & 0 & 0 & 0 \\ 0 & 0 & 0 & 0 & 0 & 0 \\ 0 & 0 & 0 & 0 & 0 & 0 \end{bmatrix}$$

F. Pre- and Post-Processing

Marc / Designer Demo Version [18] is used for pre- and post-processing. That is, the input file is prepared and the output file is interpreted using Marc / Designer Demo Version.

III. PROGRESSIVE DAMAGE ANALYSIS

50.8 x 50.8 mm laminate of ply lay-up $[0_6/90_6]_s$ with a 12.7 mm hole at the center was used to test the progressive damage analysis as described by Chang and Lessard [14,19]. The total thickness of the laminate was given to be 3.429 mm and the material properties used in the analysis can be seen in Table 1. Because of symmetry, 1/8th of the problem was modeled as shown in Fig.7. Symmetry boundary conditions were applied to the symmetry planes, that is, they were fixed in the direction of their normal vectors. Two layers of solid elements were used, one for 0_6 and one for 90_6 ply lay-ups. The analysis was conducted using Hashin failure criterion with the addition of fiber-matrix shearing failure and Yeh delamination criterion. An incremental distributed compressive load was applied from the upper edge and the progression of the damage was observed.

The analysis was conducted using three different meshes. Element and node numbers, the resulting first ply and

catastrophic failure loads of these meshes are listed in Table 2.

The course mesh of model 1 resulted with a very high catastrophic failure load when compared with the experimental data ranging between 53.16 kN and 80.10 kN with an average of 66.60 kN [19]. However, model 2 and 3 are in excellent agreement with the above experimental results. The deviations of catastrophic failure loads of model 2 and 3 from the average of experimental values are 6.9 % and 2.6 %, respectively. Further more, the damaged zone seems to be similar to the x-radiographs of Chang and Lessard [19].

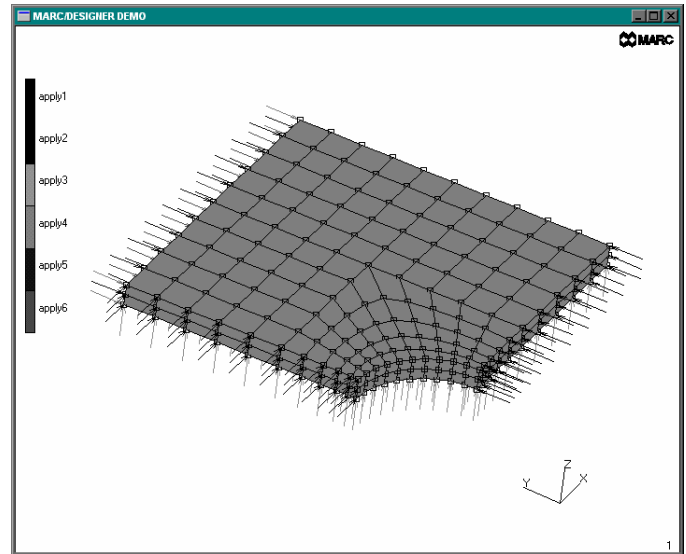


Fig.7. FE model of $[0_6/90_6]_s$ Laminate with a Hole

Table 1. Material Properties of $[0_6/90_6]_s$ Laminate

Property	Sym	Value	Unit
Longitudinal Modulus	E_1	156.4	GPa
Transverse Modulus	E_2	12.9	GPa
Out of Plane Modulus	E_3	12.9	GPa
Shear Modulus	G_{12}	7.0	GPa
Out of Plane Shear Mod.	G_{23}	3.5	GPa
Out of Plane Shear Mod.	G_{13}	7.0	GPa
Poisson's Ratio	ν_{12}	0.23	-
Poisson's Ratio	ν_{23}	0.49	-
Poisson's Ratio	ν_{13}	0.23	-
Longitudinal Tension	σ_A^+	1515	MPa
Longitudinal Compression	σ_A^-	1592	MPa
Transverse Tension	σ_T^+	44.5	MPa
Transverse Compression	σ_T^-	252.9	MPa
Longitudinal Shear	τ_A	106.8	MPa
Transverse Shear	τ_T	106.8	MPa

Table 2. Results of Progressive Damage Analysis

Mode 1	No.of Elem.	No. of Nodes	FPF (kN)	Catastrophic Failure (kN)	Error (%)
1	90	183	64.08	145.25	118.0
2	250	453	35.60	71.20	6.9
3	486	819	25.81	68.35	2.6

In all of the analyses, the first ply failure occurred in the 90₆ layer at the boundary of the hole and the failure propagated mainly in the direction of loading. The progression of the damage of model 2 can be seen in Fig.8 for 0₆ layer, together with the magnitude of the applied compressive load and combined failure index in which the highest of the failure indices were recorded. Failure index increases from light gray to black and the failure area is shown with white color. As it can be seen in Fig.8(e), Fig.8(f) and Fig.8(g), the failure propagated suddenly at the same load level. This result is obtained by redistributing the stresses after failure of elements without increasing the applied load. In Fig.8(h), the catastrophic failure of the laminate can be seen where the failed zone reached from hole to the loading edge in both layers.

IV. PINNED JOINT FAILURE

12.7 x 38.1mm and 12.7 x 50.8 mm laminates of ply lay-up [0₆/90₆]_s with a total thickness of 3.429 mm were used to conduct pin joint failure analysis. The material properties of the laminate can be seen in Table 1. A rigid pin of diameter 12.7 mm was located inside the hole with the same diameter where its center was located at 12.7 mm and 25.4 mm from the free end for the first and second laminates, respectively. The contact surface was assumed to be frictionless. Because of symmetry, one-fourth of the problem was modeled as shown in Fig.9. Symmetry boundary conditions were applied to the symmetry planes. Two layers of solid elements were used in the solution, one for 0₆ and one for 90₆ ply lay-ups. The analysis was conducted using Hashin failure criterion with the addition of fiber-matrix shearing failure and Yeh delamination criterion. An incremental distributed tensile load was applied from the lower edge and the progression of the damage was observed.

The progression of the damage of model 1 and 2, in 90₆ and 0₆ layers, can be seen in Fig.10 and Fig.11, together with the magnitude of the applied tensile load and combined failure index in which the highest of the failure indices are recorded. Failure index increases from light gray to black and the failed area is shown with white color. Deformations are magnified five times.

The failure mechanism of a pinned joint may include net-tension, bearing, or shear-out failure modes. It can be seen easily from Fig.10(a) that the damage in 90₆ layer of model 1 initiated from the upper part of the pin and propagated in the loading direction towards the upper edge (Fig.10(b), Fig.10(c)) showing the general appearance of shear-out failure mode of pinned joints.

However, as it can be seen in Fig.11, the failure mechanism of 0₆ layer of model 1 does not look like any of the failure mechanisms listed above but rather a combination of those which can be called as mixed mode failure.

The damage in 90₆ layer of model 2 initiated and developed at the upper part of the pin joint (Fig.12(a)) and propagated around the hole boundary (Fig.12(b), Fig.12(c)). The failure can be said to be in bearing failure mode. The damage of 0₆ layer initiated from the sides of the joint (Fig.13(a)) and propagated mainly towards sides (Fig.13(b), Fig.13(c)). The damage also propagated in the loading direction but did not reach the edges and therefore the failure mechanism can be said to be net-tension mode.

In both models damage was dominated by matrix tensile and matrix compressive failure mode. The distribution of these failure indices and damaged zones can be seen in Fig.14 and Fig.15. It can be seen that compressive matrix failure dominated at the upper part of the pin where compressive contact stresses are present.

V. CONCLUSION

An improvement from 25-30 % error of two-dimensional analysis of Chang and Lessard [19] to as low as 2.6 % error was obtained in the progressive damage analysis of composite laminates by conducting the progressive damage analysis of composite laminates in three dimensions, including large displacement theory, Hashin failure criterion in combination with fiber-matrix shear failure and Yeh delamination criterion and appropriate property degradation rules. Thus, it became possible not only to determine the stress distribution in three dimensions and include the out-of-plane effects in to the analysis but also to fail every element one by one in different layers and even apply suitable degradation rules for different failure modes.

By adding a contact algorithm to the analysis methodology a progressive damage analysis for pinned joints was conducted, where a contact zone exist between the nodes of pin and laminate. The analysis was conducted to observe the mode of failure of pinned joints. Expected modes of failure including net-tension, bearing, shear-out and mixed modes of failure.

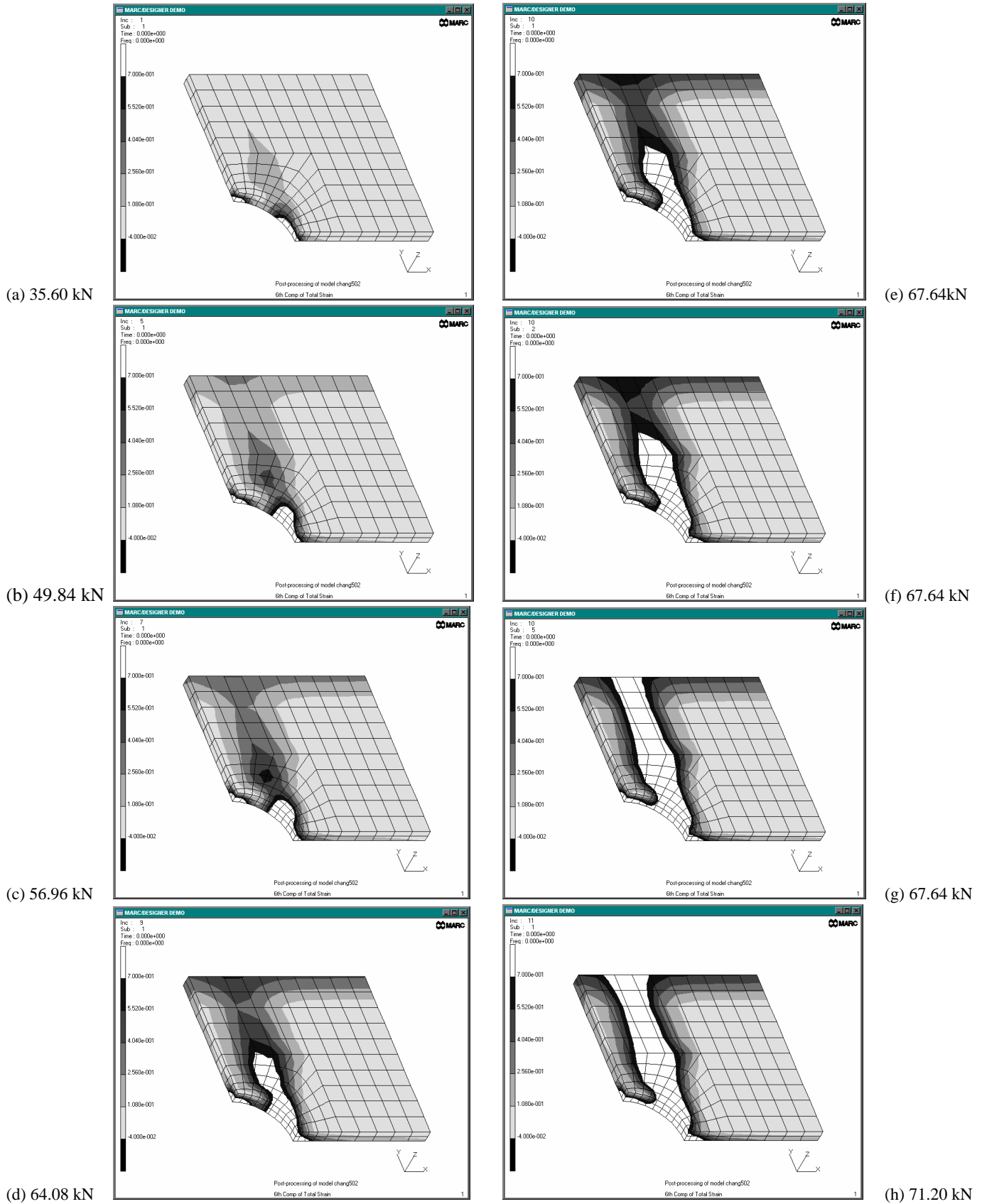
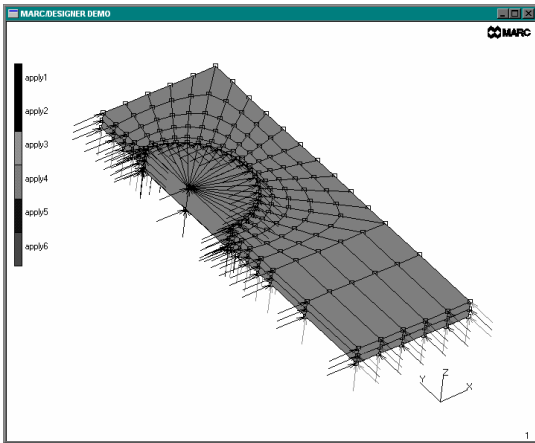
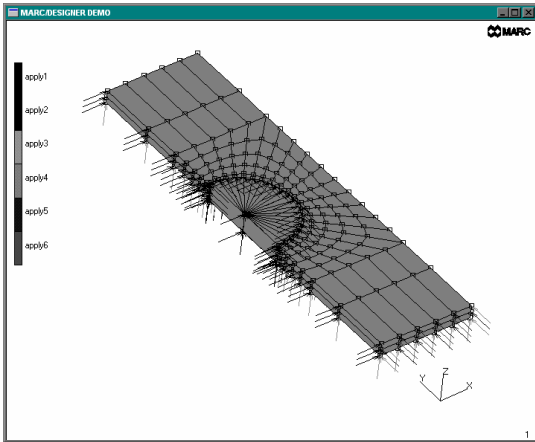


Fig.8. Progression of damage for 0_6 layer of $[0_6/90_6]_s$ Laminate with a Hole

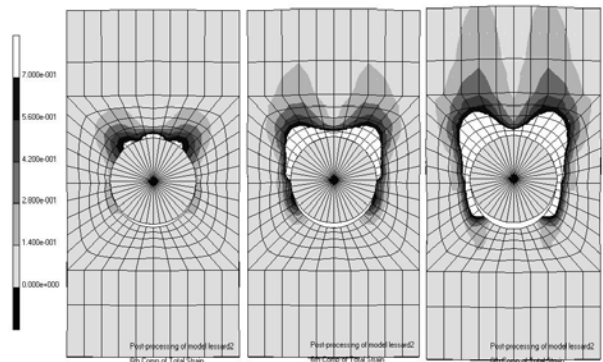


(a) Model 1



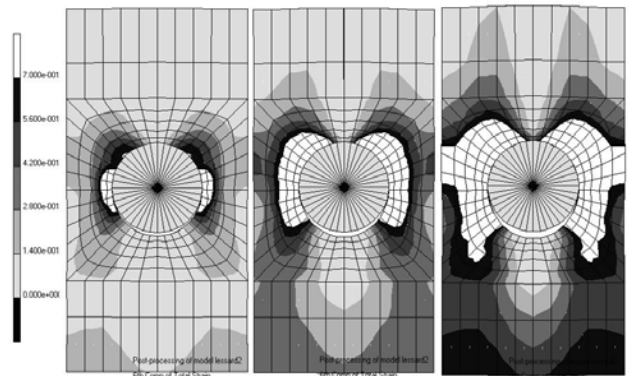
(b) Model 2

Fig.9. Finite element models for pin joint failure



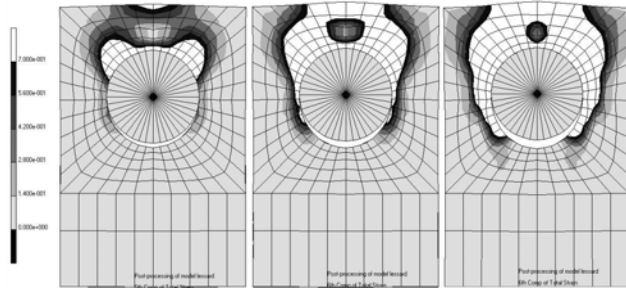
(a) 7.12 kN (b) 10.68 kN (c) 14.24 kN

Fig.12. Progressive Damage of Pin Joint (Model 2 - 90_o)



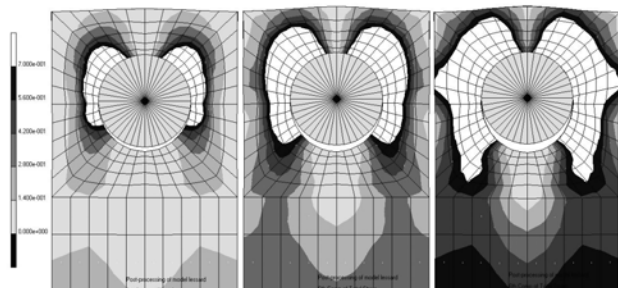
(a) 7.12 kN (b) 10.68 kN (c) 14.24 kN

Fig.13. Progressive Damage of Pin Joint (Model 2 - 0_o)



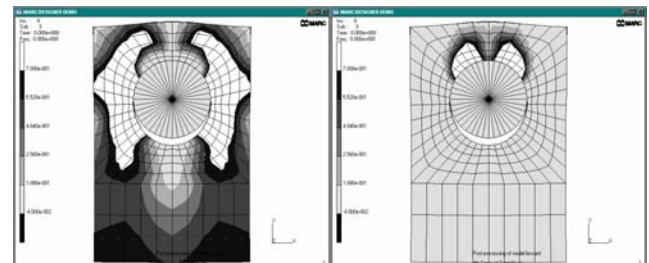
(a) 7.12 kN (b) 10.68 kN (c) 14.24 kN

Fig.10. Progressive Damage of Pin Joint (Model 1 - 90_o)

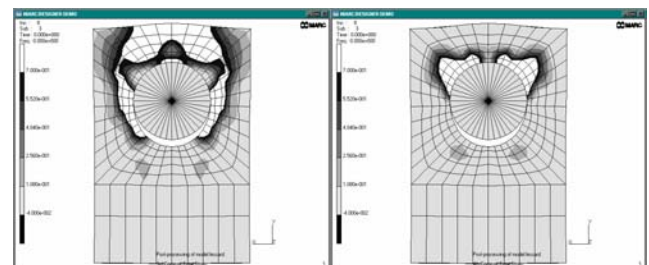


(a) 7.12 kN (b) 10.68 kN (c) 14.24 kN

Fig.11. Progressive Damage of Pin Joint (Model 1 - 0_o)

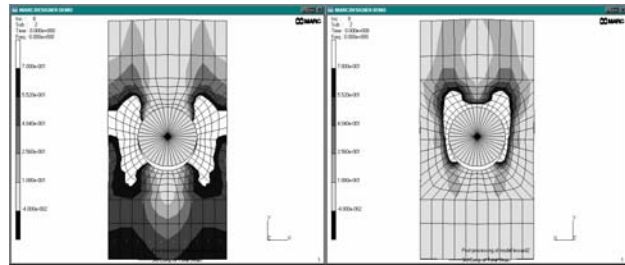


(a) Tensile Matrix (0_o layer) (b) Comp. Matrix (0_o layer)

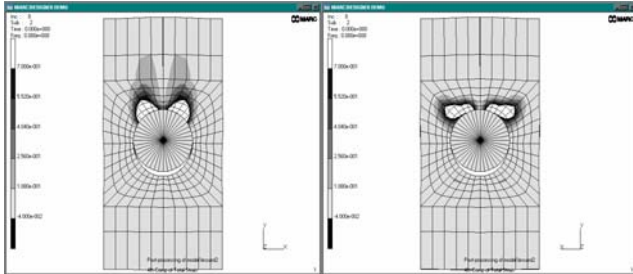


(c) Tensile Matrix (90_o layer) (d) Comp. Matrix (0_o layer)

Fig.14. Failure Index Distribution of Model 1 of Pinned Joint Analysis (14.24 kN)



(a) Tensile Matrix (0_6 layer) (b) Comp. Matrix (0_6 layer)



(c) Tensile Matrix (90_6 layer) (d) Comp. Matrix (0_6 layer)

Fig.15. Failure Index Distribution of Model 2 of Pinned Joint Analysis (14.24 kN)

REFERENCES

- [1] J.N. Reddy, *An Introduction to The Finite Element Method*, McGraw Hill, 1985.
- [2] K.J. Bathe, *Finite Element Procedures in Engineering Analysis*, Prentice-Hall Inc., 1982.
- [3] M.A. Crisfield, *Non-Linear Finite Element Analysis of Solids and Structures*, Volume 1: Essentials, John Wiley and Sons, 1991.
- [4] S.C. Charpa and R.P. Canale, *Numerical Methods For Engineers*, Second Editions, McGraw-Hill, 1988.
- [5] K.J. Bathe and S. Bolourchi, Large Displacement Analysis of Three-Dimensional Beam Structures, *International Journal for Numerical Methods in Engineering*, Vol. 14, 1979, pp. 961-986.
- [6] R. Slavkovic, M. Zivkovic and M. Kojic, Enhanced 8-Node Three-Dimensional Solid and 4-Node Shell elements With Incompatible Generalized Displacements, *Community of Applied Numerical Methods*, Vol. 10, 1994, pp 699-709.
- [7] S. Klinkel and W. Wagner, A Geometrical Non-Linear Brick Element Based on The EAS-Method, *International Journal for Numerical Methods in Engineering*, Vol. 40, 1997, pp 4529-4545.
- [8] R.M. Jones, *Mechanics of Composite Materials*, Hemisphere Publishing Company, 1975.
- [9] P.K. Mallick, *Fiber-Reinforced Composites*, Marcel Dekker Inc., 1988.
- [10] W.H. Chen and J.T. Yeh, Three-Dimensional Finite Element Analysis of Static and Dynamic Contact Problems with Friction, *Computers and Structures*, V.35, 1990, pp.541-552.
- [11] Z. Hashin, Failure Criteria for Unidirectional Composites, *Journal of Applied Sciences*, V.47, 1980, pp.329-334.
- [12] P. Papanikos et al., Progressive Damage Modeling of Bonded Composite Repairs, *Theoretical and Applied Fracture Mechanics*, V.43, 2005, pp. 189-198.
- [13] K.I. Tserpes et al., Strength Prediction of Bolted Joints in Graphite/Epoxy Composite Laminates, *Composites: Part B*, V.33, 2002, pp.521-529.
- [14] F.K. Chang and L.B. Lessard, Damage Tolerance of Laminated Composites Containing an Open Hole and Subjected to Compressive Loadings: Part I – Analysis, *Journal of Composite Materials*, V.25, 1991, pp.2-43.
- [15] W.H. Chen and S.S. Lee, Numerical and Experimental Failure Analysis of Composite Laminates with Bolted Joints under Bending Loads, *Journal of Composite Materials*, V.29, 1995 pp.12-36.
- [16] L.B. Lessard and M.M. Shokried, Two-Dimensional Modeling of Composite Pinned-Joint Failure, *Journal of Composite Materials*, V.29, 1995 pp.671-697.

[17] Y. Xiao and T. Ishikawa, Bearing Strength and Failure Behavior of Bolted Composite Joints (part II: modeling and simulation), *Composites Science and Technology*, V.65, 2005, pp.1022-1031.

[18] *Marc / Designer Demo Version, Reference Manual*, Marc Analysis Research Cooperation, Palo Alto, CA, 1995.

[19] F.K. Chang and L.B. Lessard, Damage Tolerance of Laminated Composites Containing an Open Hole and Subjected to Compressive Loadings: Part II – Experiment, *Journal of Composite Materials*, V.25, 1991, pp.44-64.

Ali Evcil received B.Sc., M.Sc. and Ph.D. degrees in mechanical engineering from Middle East Technical University, Turkey, in 1990, 1993 and 2000, respectively.

Since 2001 he has been working as an Assistant Professor at Near East University, Nicosia, Cyprus. He was Vice-Chairman from 2001 to 2003 and since 2003 he is Chairman of Mechanical Engineering Department at the same university.

Dr. Evcil's current research interests include finite element analysis, viscoelastic materials, composite materials, progressive damage, biomechanics. Contact him at: Department of Mechanical Engineering, Near East University, Nicosia, Cyprus; evcil@neu.edu.tr.